Int J Appl Earth Obs Geoinformation 73 (2018) 300–312

Contents lists available at ScienceDirect

Int J Appl Earth Obs Geoinformation

journal homepage: www.elsevier.com/locate/jag

A robust object-based woody cover extraction technique for monitoring mine site revegetation at scale in the monsoonal tropics using multispectral RPAS imagery from different sensors

Timothy G. Whiteside*, Renée E. Bartolo

Environmental Research Institute of the Supervising Scientist, Darwin, NT, 0820, Australia

ARTICLE INFO

Keywords:
Rehabilitation assessment
RPAS
UAV
Time series
Ultra-high resolution
Woody cover

ABSTRACT

Revegetation success is a key element of mine site rehabilitation. A number of criteria related to mine site close-out are associated with revegetation. The monitoring of mine site revegetation efforts have traditionally been undertaken using field-based plot or transect methods. Often the sampling design for this monitoring is limited due to resource constraints, therefore reducing the statistical power of the data and missing information over most of the mine site. The recent advances in Remotely Piloted Aircraft Systems (RPAS) technology for remote sensing enables the collection of appropriate scale data over entire mine sites reducing the need for sampling and eliminating potential bias. This paper describes an object-based technique for extracting woody cover and estimating proportional woody cover from RPAS imagery over the rehabilitated Jabiluka mine site located in the tropical north of Australia. The technique was tested on three data sets that covered three different dates, two different sensors, and two different processing methods. Overall woody cover detection accuracies from each data set were over 95%. Proportional woody cover derived from the technique showed strong linear relationships with manually estimated cover ($r^2 > 0.88$). This study shows that the technique is robust and works with a range of RPAS data sets and enables at scale analysis of woody cover change between dates. The technique will be an important component of ongoing monitoring of mine site revegetation in the region.

1. Introduction

The success of mine site rehabilitation is typically assessed by comparing the progress of revegetation and landform condition against nearby reference sites that are analogous to the pre-mining condition (Gravina et al., 2011; Lechner et al., 2012a). Observations and measurements of a number of biophysical parameters over time are used to assess whether the status of the rehabilitation is following a preferred trajectory that can meet defined closure criteria. Key to any monitoring scheme is a sampling design capable of detecting significant change (Field et al., 2007). Standard procedures for the monitoring of mine site rehabilitation generally involve observations of a number biophysical parameters over time within a number of sample sites (including field plots, transects or quadrats) that are intended to be representative of the larger landscape in which they are located. The number of sample sites, where they are located on a rehabilitated site and surrounds, and how often they are sampled can be limited due to access and resource constraints. Thus the spatial and temporal coverage of the sites may be minute when compared to the entire area under rehabilitation. Therefore, the limited sampling scale of field data may not capture the spatial and temporal variation of biophysical parameters relevant to vegetation growth and condition across the entire site at the most appropriate scale. Additionally, such monitoring may not have the statistical power to adequately describe phenomena and make informed decisions (Lechner et al., 2012a). There needs to be sufficient sampling to ensure replication to increase confidence of detecting an effect. For example, a limited scale of sampling may show significant differences in the spatial heterogeneity and biodiversity within the same vegetation community (Lechner et al., 2012b). Therefore, the greater the intensity of sampling the better information spatially and temporally, however comprehensive field surveys are resource intensive, and in tropical areas are time-consuming, financially expensive, and logistically challenging (Gardner et al., 2008). In addition, quantitative measures of structure and function at the plot level may not scale up to landscape, primarily due to increasing the heterogeneity associated with larger areas.

Remote sensing technologies have been used for environmental monitoring purposes at the continental (Mildrexler et al., 2007),

* Corresponding author.
E-mail address: tim.whiteside@environment.gov.au (T.G. Whiteside).

https://doi.org/10.1016/j.jag.2018.07.003
Received 22 March 2018; Received in revised form 2 July 2018; Accepted 2 July 2018
Available online 10 July 2018

Table 1
Spatial and temporal quality for methods of collecting data over a mine site in remote tropical regions.

Data collection method	Spatial resolution	Spatial coverage	Temporal resolution
Field-based collection	High	Low[b]	Low[b]
Remotely Piloted Aircraft[a]	High	Medium/High	High
Piloted Aircraft[a]	High	High	Low[b]
Satellite[a]	Low[c]	High	High/Medium[d]

[a] Remote sensing techniques.
[b] Cost is a limiting factor for remote areas.
[c] Cost is a limiting factor for higher resolution imagery.
[d] Cloud cover is a limiting factor for tropical areas.

regional (Hutley et al., 2011) and local or catchment (Whiteside and Bartolo, 2015) scales. Remote sensing data can provide complete coverage of a site, however temporal and spatial resolution are dependent upon the sensor and platform. Subsequently, some data may not be suitable for monitoring mine site rehabilitation. Table 1 summarises the spatial and temporal aspects of various data collection methods for monitoring of mine site revegetation. As mentioned previously, due to resource and logistical constraints, spatial coverage and temporal resolution of field-based data are typically low. The temporal resolution for piloted aircraft data acquisition is influenced by availability and deployment costs, particularly in remote areas. Satellite data whilst providing full spatial coverage, is limited in spatial resolution due to cost and even high spatial resolution satellite data are not able to detect revegetation in its early stages of development. In addition, temporal resolution can be limited due to cloud cover for much of the year particularly in the tropics.

Recent advances in active and passive sensor technology have resulted in smaller lightweight sensors. Remotely piloted aircraft systems (RPAS), also known as unmanned aerial systems (UAS) or drones, have been used successfully as platforms for multispectral and hyperspectral remote sensing of land surfaces including vegetation (Laliberte et al., 2011a; Sankey et al., 2017). Data acquisition using RPAS-based sensors is possible at sub-decimetre spatial resolution and at sub-diurnal temporal resolutions (Laliberte and Rango, 2009; d'Oleire-Oltmanns et al., 2012; Harwin and Lucieer, 2012). The capacity of RPAS technology for undertaking high resolution and repeatable data acquisitions makes them ideal for analysis of phenomena at high temporal and spatial resolution over site scales (~200 ha). Imagery captured using RPAS has been used to derive rangeland vegetation attributes including, growth form, proportional cover and species (Laliberte and Rango, 2009; Laliberte et al., 2010), for mapping of vegetation condition within riparian forests (Dunford et al., 2009) and as a low cost method of surveying and mapping of forests and biodiversity at local scales in southeast Asia (Koh and Wich, 2012). The key advantage of a remotely piloted aircraft (RPA) platform is the ability to fill a scale niche with respect to spatial and temporal resolution between field sampling (very high spatial resolution but limited coverage) and satellite observations (with full coverage but low spatial or temporal resolution) (Laliberte et al., 2011a; d'Oleire-Oltmanns et al., 2012; Lucieer et al., 2012; Pádua et al., 2017). In addition, RPAS can be flown and imagery acquired on-demand making it possible to capture imagery at a frequency effective for monitoring (i.e. the imagery can be hyper-temporal) (Laliberte et al., 2011a; Lucieer et al., 2012). In addition, data can be collected covering an entire site which eliminates many of the issues associated with sampling design and bias.

RPAS-derived data have proven to be useful for the characterisation and assessment of vegetation communities including forests (Getzin et al., 2012; Puliti et al., 2015), upland swamps (Lechner et al., 2012b), arid rangelands (Breckenridge et al., 2011; Laliberte et al., 2011b; McGwire et al., 2013), wetlands (Chabot and Bird, 2013) and aquatic vegetation (Husson et al., 2014). In addition, RPAS have been used for the identification and mapping of weeds in agricultural (López-Granados, 2011; Peña et al., 2013; Rasmussen et al., 2013), rangeland (Hung and Sukkarieh, 2013) and aquatic landscapes (Chabot et al., 2017). Revegetation efforts have also been the subject of analysis using RPAS data in riparian areas (Dufour et al., 2013) and pipeline rights of way (Booth and Cox, 2009). High temporal resolution RPAS imagery was used for monitoring phenology of floodplain vegetation (Van Iersel et al., 2016). The radiometric properties of RPAS acquired data have been used to detect plant condition including water stress (Suárez et al., 2010; Stagakis et al., 2012; Zarco-Tejada et al., 2012), and have correlations with a number of biophysical properties including leaf area index (LAI) (Lelong et al., 2008; Hunt et al., 2013; Lu et al., 2017).

Spectral information within image bands has been combined with hyper-resolution digital surface models (DSMs) derived from the overlapping RPAS imagery to enable further characterisation of land cover. Lucieer et al. (2012) used a micro-RPA for ultra-high resolution multisensor observations of Antarctic moss beds. This included deriving a topographic wetness index from a 2 cm resolution surface model, and NDVI (a surrogate of photosynthetic activity) from multispectral imagery. RPA technology has also been used for mapping vegetation above an underground mine site. In particular, the characterisation of swamps affected by subsidence related to underground coal mining using both RGB imagery and the DSM derived from the overlapping imagery (Lechner et al., 2012b). In addition, species specific maps were created by classifying CIR imagery over the above shrub swamps in southeast Australia (Strecha et al., 2012). RPAS-derived DSMs have also been used for developing canopy height models (Lisein et al., 2013) and the characterisation of woody plant structure in savanna has also been investigated using RPAS derived photogrammetric point clouds (Mayr et al., 2017).

One remote sensing derived attribute suitable for determining the success of mine site rehabilitation is woody cover. Woody cover can be defined as the 2D area covered by tree crowns in an image. Spatial measures of woody cover can be used to indicate a number of ecosystem services such as variability in water balance and primary production (Simioni et al., 2003), and as habitat for animals (Curran and Foody, 1994; Murwira and Skidmore, 2006). Measures of woody vegetation cover density over time can also be used to assess the growth of plants on revegetated mine sites during the rehabilitation phase. Therefore, woody cover density is a key criterion for rehabilitation monitoring and is linked to key biophysical vegetation measures such as foliage projected cover (FPC) (Specht, 1981) or leaf area index (LAI) (Chen et al., 1997) which are indicators of ecosystem services such as photosynthesis. Green woody cover is an attribute that is readily acquired from high spatial resolution remotely sensed data such as aerial photography and is highly correlated to field-based measures such as FPC (Staben et al., 2016). FPC is calculated as the percentage of a sample site covered by the vertically projected green foliage of woody vegetation (Specht, 1981). LAI is defined as one half of the total green leaf area per unit ground surface area (Chen et al., 1997). FPC has allometric relationships to LAI and other biophysical parameters such as stand basal area (Armston et al., 2009). The collection of woody cover data at high spatial and temporal resolution over an entire site can assist with differentiating localised or short term variability over longer term change (Bao et al., 2014). In addition, woody cover density can be compared against information from reference sites to assess progress towards closure of a rehabilitated mine site. This monitoring of performance and viability of revegetation, particularly in the early stages, can allow for intervention if progress is not along a defined trajectory. Empirical relationships between green foliage measures and spectral vegetation indices are well described in the literature (Gitelson, 2004). The most widely used index is the normalised difference vegetation index or NDVI (Rouse et al., 1973) which is strongly correlated to vegetation productivity (Reed et al., 1994).

Vegetation cover analysis from RPAS data has been undertaken using geographic object-based image analysis (GEOBIA) classification techniques (Laliberte and Rango, 2009; 2011; Kelcey and Lucieer, 2013). Benefits of using object-based methods for classification include: the mitigation of the effects of within field heterogeneity (salt and pepper effect); the image segmentation creates objects that can represent surface features; and the ability to apply context related features such as shape, texture and spatial relationships (Blaschke, 2010). GEOBIA techniques are usually applied where the phenomena being classified are much larger than the ground sample distance (GSD) within the imagery and consist of many pixels such as land cover classifications.

This study investigates the potential for multispectral RPAS data combined with GEOBIA to capture biophysical information, in particular, proportional woody cover to enable the monitoring of revegetation efforts on mine sites. To test the robustness of the technique, it was applied across sensors with different radiometric characteristics, and imagery created using different processing methods and different GSD.

2. Method

2.1. Study site

The study site was the Jabiluka mine site (12° 29′56″ S, 132° 54′50″ E), located within the Jabiluka mineral lease belonging to Energy Resources of Australia (ERA) (Fig. 1a). The mineral lease is surrounded by the World Heritage listed Kakadu National Park. The climate is wet dry monsoonal tropical with an intense wet season (December to March) when most of the annual rainfall occurs and a longer slightly cooler dry season (April-November) with little to no rainfall. The site is situated on the edge of the Arnhem Land escarpment and the vegetation is mostly savanna matrix discontinuous trees and annual grasses, with rocky outcrops. Although the mine was never operational, an underground incline, a water management pond and a compacted area for processing and stockpiling were constructed (Fig. 1b). Rehabilitation works undertaken by ERA on the site commenced in 2003 with initial work undertaken on the hard stand area as well as the backfilling of the incline. Between 2003 and 2008, 3690 tubestock (seedlings propagated

Table 2
Number of tubestock planted at Jabiluka per area in November–December 2013.

Area	Approximate size (ha)	Number of Seedlings
A	1.7	858
B	2.2	15
C	0.6	289
D	1.2	907
E	1.6	909
F	2.0	602
G	0.6	5

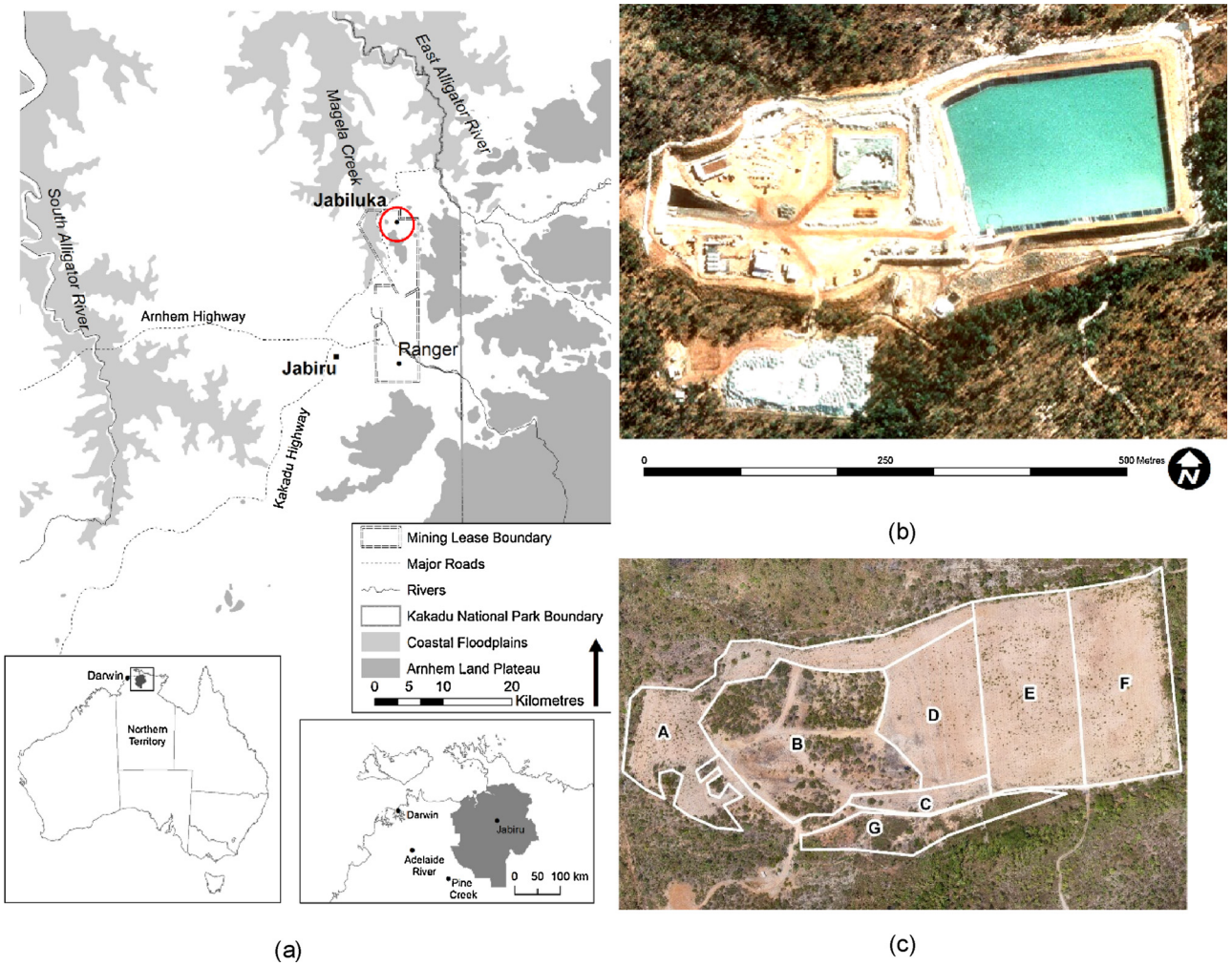

Fig. 1. Location of the study site (a), subset of an air photo over Jabiluka mine site 4 November 1999 (b), and planting areas draped over RGB mosaic for 23 December 2014 (c).

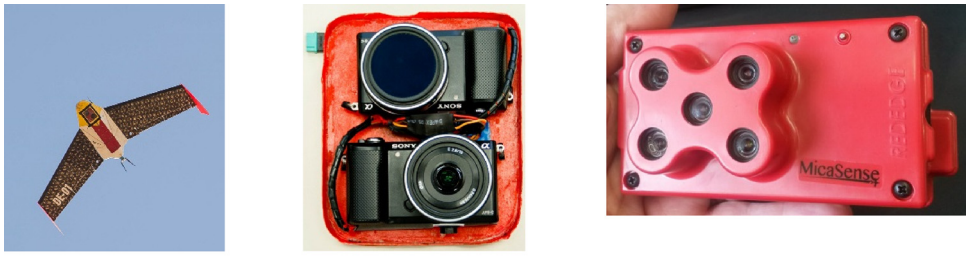

Fig. 2. (a) The Swampfox RPAS, including the aircraft and GCS; (b) the Sony sensor system, NIR camera (top) and RGB (bottom), and (c) MicaSense RedEdge multispectral sensor.

in a tube) were planted. ERA conducted further rehabilitation works commencing in 2013, including the removal of the pond, and shaping of the surface. Initial plantings of approximately 3600 tubestock occurred across the site during November and December 2013; with a further 4500 tubestock introduced in November 2014 and 500 in March 2015. Fig. 1c shows the planting areas and the numbers of initial plantings per area are listed in Table 2. The site decreases in elevation from west to east. Since the 2014 surface shaping, material (mostly sand) has been removed principally from area D and deposited in areas E and F. This movement has left waste rock substrate very close to and occasionally exposed on the surface in area D. Given only 5 tubestock were planted in area G, the area was excluded from this study.

2.2. Platform and sensors

The RPAS used for this study was a Swampfox X5 flying wing (Fig. 2a) from Skycam UAV (www.kahunet.co.nz). The aircraft has a 2.3 m wingspan and construction consists of a Kevlar composite fuselage with wings of expanded polypropylene foam covered with a reinforced lamina. The airframe has a maximum all up weight of 4.8 kg, a payload capacity of 1.1 kg, and is propelled by a 750 KV brushless electric motor powered by 10 Ah 14.4 v batteries providing a maximum 50 min flight time at a cruise speed of 60 kph. The onboard flight controller uses sensors to enable remotely piloted flight including GNSS (Global Navigation Satellite System), inertial measurement unit (IMU), barometer, and airspeed sensor. Remote piloting was undertaken using communications between the RPA and the ground control station (GCS) via a 900 MHz radio link.

The payload sensor system (Fig. 2b) on board the RPAS for the first two flights consisted of two Sony NEX-5 cameras. For the 23 December 2014 flight, both cameras were Sony NEX-5R, and for the 10 July 2015 flight, both cameras were Sony NEX-5 T. For each flight, one of the cameras was a standard RGB while the other was modified to capture near infrared data. The modification removed the internal Beyer filter which prevents NIR light transmission through to the sensor, and the inclusion of a high pass filter allowing light only above 720 nm to transmit through to the sensor. Bryson et al. (2013) used a similar system with the same model camera and calculated the response curves for the bands captured (Table 3). Settings for the Sony cameras included F-stop set at f/4.5, exposure time 1/1000sec, ISO setting 400, focal length 16 mm (or equivalent 35 mm focal length of 24 mm). The Complimentary Metal-Oxide-Semiconductor (CMOS) sensor resolution was 16 megapixels (MP, 4928 × 3276 pixels).

Table 3
Expected peak responses of Sony NEX 5 colour and NIR converted cameras (from Bryson et al., 2013). Bandwidth is measured at full width at half maximum (FWHM).

	Blue	Green	Red	NIR
Peak response	470 nm	530 nm	606 nm	740 nm
Approx. bandwidth FWHM	60 nms	60 nm	60 nm	55 nm

Table 4
Spectral information for the MicaSense RedEdge multispectral camera. Bandwidth is measured at full width at half maximum (FWHM).

Band Number	Band Name	Centre Wavelength (nm)	Bandwidth FWHM (nm)
1	Blue	475	20
2	Green	560	20
3	Red	668	10
4	Near Infrared	840	40
5	Red Edge	717	10

For the third flight on 1 June 2016, data were captured using a MicaSense RedEdge (www.micasense.com) multispectral camera (Fig. 2c). The MicaSense RedEdge has five narrow band sensors between 475 and 840 nm (Table 4). Data was captured at a frame rate of 1 photo per 1.5 s along with GPS (time, heading, location and altitude) and aircraft attitude information (pitch, roll and yaw). Raw sensor data captured as 12-bit TIFF files. The pixel resolution of each sensor is 1280 × 960 (1.2 M P). Focal length was 5.5 mm (or equivalent 35 mm focal length of 39.7 mm), f-stop was f/2.5, ISO setting at 800 and exposure time was less than 1/700 s.

2.3. Flight/mission details

The first step in the image acquisition and processing workflow (Fig. 3) was undertaking the flights to collect imagery. Details for each flight are provided in Table 5, include date and times and number of images captured. Frame rate for each flight was 1.5 s ensuring 75%

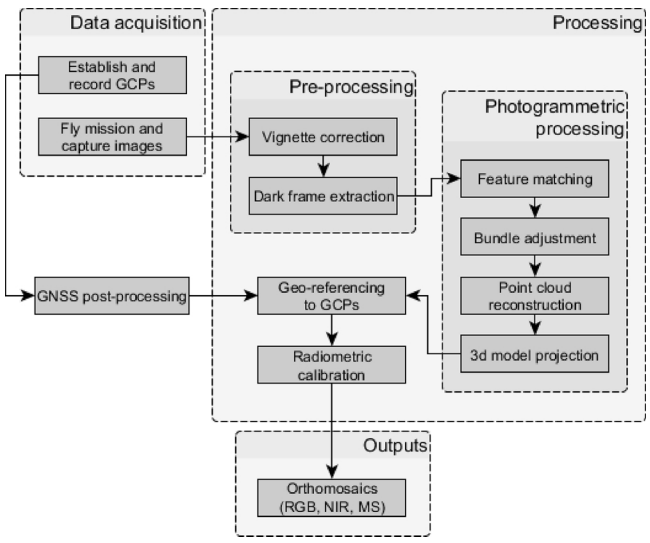

Fig. 3. Overview of the image acquisition and data processing workflow.

Table 5
Flight details include dates, times and number of images captured per camera. * MicaSense RedEdge has one camera per band, value in parentheses is total number.

Date	Start time	End time	Sony RGB	Sony NIR	MicaSense*
23 December 2014	12:52	13:22	460	460	
10 July 2015	12:15	12:35	364	364	
1 June 2016	12:28	12:49			445 (2225)

forward overlap at 120 m altitude. Side overlap was 60% for flights with Sony cameras and 75% for the MicaSense flight. For the first two flights, the autopilot created a photolog recording the time, heading, location and altitude, and aircraft attitude information (pitch, roll and yaw) for each photo. For the final flight, the MicaSense camera was directly connected to a Global Navigation Satellite System (GNSS) receiver recording time, heading, location and altitude in the metadata for each image.

2.4. Field data

Six ground control points (GCPs) were marked on the ground surface and the location of each was recorded using differential GNSS and post-processed to sub-decimetre accuracy (Fig. 4a). In addition, for the purposes of radiometric calibration, pseudo-invariant target panels consisting of light and dark reference material of near-Lambertian properties with known spectral responses (Pfitzner et al., 2010) were also located across the study site. For the MicaSense RedEdge camera, several images per band of the proprietary calibration panel (Fig. 4b) were captured immediately prior to the flight. The Micasense RedEdge has a downwelling light sensor to measure solar irradiance in the 5 bands at the time of each capture, however this was not used as it was unavailable at the time of the flight.

2.5. Image processing and outputs

Pre-processing involved correction for potential systematic image errors including lens distortion and sensor pixel variability. The two processes undertaken were vignetting correction and dark frame extraction. No corrections for the effects of bidirectional reflectance distribution function (BRDF) were undertaken due the effect of terrain on reflectance being assessed as negligible for the time of day flights were undertaken.

2.5.1. Dark frame correction

Dark frame correction was conducted to correct for sensor pixel variability using a per-pixel correction factor lookup table (LUT) based upon a dark frame image created from an average of several images taken with the camera in an unlit darkroom with the lens cap on.

2.5.2. Vignetting correction

Vignetting is the radial attenuation of brightness away from the image centre. Causes of vignetting include optical properties of the lens, and the geometric and mechanical obstruction of light. Vignetting in the Sony imagery was compensated for using the flat-field correction method (Kelcey and Lucieer, 2012). Flat field correction was undertaken using a per-pixel correction factor LUT based upon a camera specific image of a uniform spectrally-homogeneous Lambertian surface (the flat field). For the flat-field, a 25 × 25 cm Spectralon® 99% reflectance white spectral reference panel was used under diffuse multiple quartz-tungsten-halogen lamplight in a darkroom. All camera settings for the flat field image were the same as used during flights as these parameters affect vignetting. An image of the flat-field displaying the vignetting effect was then used to create the correction factor LUT using a quadratic polynomial function. The correction factor LUT for each camera was then applied to the original images captured by the same camera to create the flat field images (Fig. 5).

2.5.3. Photogrammetric processing

The 23 December 2014 photos were processed into an orthomosaic by a commercial aerial mapping company, Aerometrex Pty Ltd (www.aerometrex.com.au), using proprietary photogrammetry techniques and multiple software. The orthomosaic (consisting of NIR, Red and Green bands) was provided as tiles in 8-bit TIFF format. The photogrammetric software used for processing the corrected RPAS photos from the other two flights into orthomosaics was Pix4DMapper Pro (pix4d.com). The software uses a workflow of processes to produce orthomosaics from the RPAS images. For the 2015 flight, the data input into the processing were the pre-processed photos, the UAV photo log and GCP coordinates. For the 2016 flight, MicaSense photos with updated EXIF data (position and attitude) along with a file with the GCP coordinates.

The first process involved automatic tie point matching, where multiple corresponding locations were automatically identified in overlapping photos. These tie points were then used to geo-rectify the photos. Observations from the tie point matching were used for bundle adjustment, creating internal camera parameters and external image parameters to geometrically align the imagery. After the images are aligned the next process was point cloud densification to enable a more detailed surface model. The dense point cloud was used to reconstruct the surface via a triangular irregular network (mesh). The mesh was the basis for a digital surface model (DSM). The DSM and adjusted images are then used to create an orthoimage of the site. Post-processing, the ground sample distance (GSD) for the Sony image mosaics is 3 cm for

Fig. 4. (a) One of the ground control points and radiometric calibration targets. (b) The Micasense RedEdge radiometric calibration panel captured pre-flight for the NIR band.

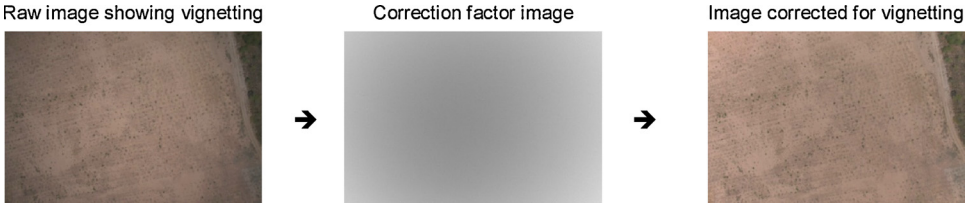

Fig. 5. Vignetting correction process using the flat field method.

2014 imagery and 3.4 cm for the 2015 imagery. For 2015, 724 out of 728 images (both NIR and RGB) were calibrated with a median of 5768 tie point matches per calibrated image. The mean root mean square error (RMSE) for the georeferencing was 0.04 m. Post-processing GSD for MicaSense RedEdge imagery is 8.3 cm. For the 1 June 2016 processing: 2220 out of 2225 images were calibrated with a median of 10,668 tie point matches per calibrated image. The mean RMSE for the georeferencing was 0.033 m. Although no geometric accuracy information was provided with the 23 December 2014 commercially produced orthomosaic, an analysis of the location of the GCPs in the mosaic produced a mean RMSE of 0.0352 m. A locational comparison of 20 readily identified features between the 2014 and 2015 mosaic provided a mean RMSE of 0.24 m.

It is noted here that the DSMs produced during the Pix4D Mapper processing were not used in any of the subsequent woody cover analysis due to problems with detecting sufficient points representing trees on the site (see Discussion). In addition, a DSM was not provided by Aerometrex for the December 2014 image.

2.5.4. Radiometric correction of mosaics

For all data sets, at sensor digital numbers were converted to surface reflectance. For the Sony RGB and NIR imagery from the first two dates, radiometric correction involved the use of 5–6 radiometric reference panels, as shown in Fig. 4a, distributed across the site. Correction involved regression fitting between the mean DN value of pixels representing the calibration panels for each band and the known spectral response of the panels using the empirical line method based upon 2nd order polynomial equations (Smith and Milton, 1999). For the MicaSense RedEdge imagery, reflectance mosaics for each of the five bands were created within the Pix4DMapper software using input from the images taken of the MicaSense calibration panel, and the application of the calculated albedo parameter for each band. The albedo parameters are specific to the panel and provided by MicaSense. All mosaic outputs post reflectance were 32-bit TIFF format.

2.6. Ancillary data - vector layers

Three vector layers were incorporated into the analysis: (1) a boundary of the area under rehabilitation used for restricting the extent of investigation; (2) the planting areas as assigned by ERA; and (3) a grid of 10 × 10 m squares providing an arbitrary unit of analysis of a finer scale than the planting areas suitable for quick analysis of change in cover.

2.7. Image analysis

The technique to extract woody cover from the study site used an object-based approach within eCognition Developer software version 9.2. The main focus of the technique was establishing woody cover objects based on a threshold of a spectral vegetation index (Fig. 6). The first step was the creation of an NDVI layer based upon the NIR and Red bands from the data set. To reduce within field noise, the NDVI layer was then subjected to a low pass Gaussian Blur filter based upon a 5 × 5 kernel.

Table 6 provides details of process parameters use in the woody cover analysis of each data set. The first object level (L1) was created using the boundary of the rehabilitated areas used to restrict the woody

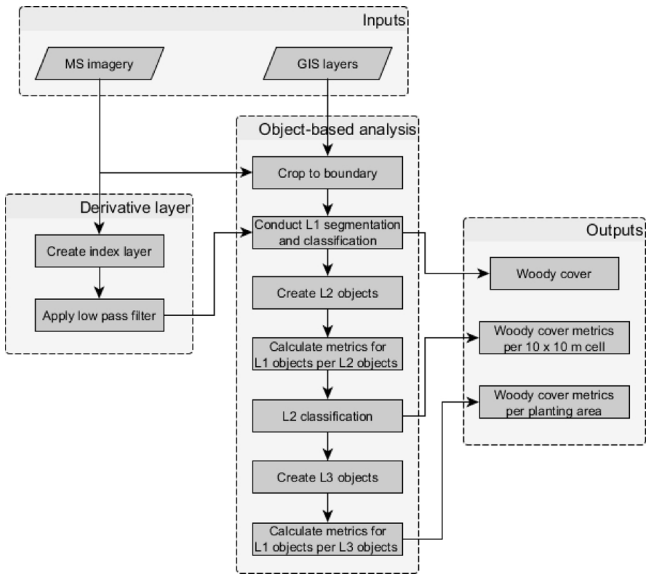

Fig. 6. Image analysis workflow.

cover extraction to this area. The initial segmentation and classification step at L1 identified green woody cover based upon thresholding the filtered NDVI layer. The value for the NDVI threshold was determined by sampling the NDVI values of pixels within more than 20 tree crowns in each image and using the lowest value detected. Due to sensor variation between flights and the method of radiometric calibration, a slightly different value was measured for the threshold for 2016 compared to the other dates.

Using a technique based upon thresholding can result in areas of dense and overlapping canopy woody cover being over-estimated. Therefore, rules were created to firstly to identify these areas or 'chunks', objects greater than 300 m^2 that consisted of multiple plants and background, and the subsequent re-segmentation of the chunks using a higher threshold value. The removal of small spurious objects that were uncertain as to whether they were woody plants or not was also undertaken by applying a rule to eliminate objects that were less than 100 cm^2.

In the object level (L2) above the woody cover level (L1), a grid of nominal units for analysis was created. In this instance, the nominal unit was a 10 x 10 m square to enable analysis of proportional cover at a scalable unit below the extent of planting areas but at a size for detecting localised change relevant to strategic intervention. In the third or top level of the hierarchy (L3), objects were created based upon the planting area vector layer.

For objects in both the L2 and L3 levels, the relative area of L1 objects was calculated along with the number of L1 objects and mean size of L1 objects. The classifications of the L2 nominal units and L3 planting areas are based upon proportional cover. L2 classes were 'Less than 1%', '1–10%', '11–20%', '21–30%', '31–40%', '41–50%' and 'Greater than 50%'. L3 classes were '1–10%', '11–20%', '21–30%', '31–40%', and '41–50%'.

Table 6
Summary of processes and parameters used for woody cover extraction and analysis.

Level	Operation	Algorithm/Object metrics	Parameter	Value/s
L1	Segmentation and classification of woody cover	Multi-threshold segmentation	Image layer Threshold	NDVI > 0.20 (2014) > 0.20 (2015) > 0.25 (2016)
L1	ID cover chunks within woody cover	Assign class / area	Object size greater than	300 m^2
L1	Re-segment chunks to woody cover	Multi-threshold segmentation	Image layer Threshold	NDVI > 0.30 (2014) > 0.30 (2015) > 0.35 (2016)
L1	Remove spurious objects	Remove objects / area	Object size less than	100 cm^2
L2	Create 1 ha grid	Chessboard segmentation	Size Thematic layer	10000000 pixels 1 ha grid
L2	Classify proportional cover	Assign class / Relative area of sub-objects	Use class	< 0.1, 01-0.2, 0.21-0.30, 0.31-0.40, 0.41-0.50, > 0.50
L3	Create planting areas	Chessboard segmentation	Size Thematic layer	10000000 pixels Planting areas
L3	Classify proportional cover	Assign class / Relative area of sub-objects	Use class	< 0.1, 01-0.2, 0.21-0.30, 0.31-0.40, 0.41-0.50, > 0.50

2.8. Validation of woody cover detection

A method widely used to assess the accuracy of the classification of ultra-high spatial resolution data such as acquired using RPAS is to compare the approach to what is observed in the imagery (d'Oleire-Oltmanns et al., 2013; Chabot et al., 2017). Due to this resolution, objects on the ground consist of many pixels and are generally readily identifiable. Additionally, field-based observations are likely to be less spatially accurate as observations taken from the imagery. To achieve such accuracy, the amount of resources required to collect extensive reference data may not be viable. For this study, 125 points were randomly generated within each of the planting areas. Each point was visually assessed from the imagery and classified based upon the underlying condition identified in the imagery: plant or no plant. The identified class for each point was then compared to the class prescribed by the object-based analysis and results presented in a confusion matrix providing overall, Producer and User accuracies (Congalton and Green, 2009).

2.9. Validation of proportional cover

A visual assessment of percentage woody cover was undertaken as a reference dataset for the validation of the proportional cover. The assessment was based upon methods for manually extracting woody cover from high resolution aerial photography (Fensham et al., 2002; Staben et al., 2016). Within the object level of 100 m^2 squares, fifty squares were randomly selected. Within each of the randomly selected squares, a graticule of 10 × 10 points spaced 1 m apart horizontally and vertically was created. Woody cover was visually assessed at each point (binary yes or no). The number of points assessed as yes were tallied providing a percentage of woody cover per square. The visual cover percentages were then plotted against the object-based proportional cover for each square and r^2 value determined.

3. Results

3.1. Photogrammetric results

False colour near infrared photogrammetric results for the three mosaics are shown in Fig. 7a–c. Visual assessment of these mosaics shows an increase in the size of the vegetation over the eastern and western portions (planting areas A, E and F) of the mine site between the dates. Less successful is planting area D and the southwest section of planting area B.

3.2. Classification results

Woody cover maps for all three dates are shown in Fig. 7d–f. A gradual increase in woody cover was evident over the site between the dates for areas A, E and F as well as the eastern portion of D. This is consistent with the expected initial growth of the planted tubestock. Planting area B showed little visible change due to being mature coverage and having minimal plantings.

Accuracy assessments for woody cover classification for each date are shown in Tables 7–9. All three classifications show a high level of accuracy. For the 2014 woody cover, classification overall accuracy was over 98%. User accuracy and Producer accuracy for the woody cover class were 96% and 97% respectively. Omission typically occurred where plants had sparse canopies and background reflectance had influenced the NDVI value for that plant (Fig. 8a). A small number of areas are apparent where the ground cover with high NDVI values had been commissioned into the Woody cover class (Fig. 8b) however this area was not great. Classification overall accuracy for 2015 was almost 96%. User accuracy and Producer accuracy were 92% and 93% for the woody cover class respectively. As for the 2014 accuracy assessment, omission errors in 2015 typically occurred where plants have sparse canopies and the influence of background reflectance has reduced the NDVI value for those pixels representing that plant. For 2016, the classification had an overall accuracy of 94.8% making it the least accurate of the three. User accuracy and Producer accuracy were 95% and 92% respectively. Omission errors included small plants, and those with sparse canopies. The slightly lower accuracy may be due to imagery for this date having a larger GSD.

Tables 10–12 provide a breakdown of the accuracies per planting areas for the three dates. For the 2014 woody cover classification, the overall accuracies for each area were 96% or above. Areas D and E had the lowest User Accuracies (83% and 80% respectively) which are likely attributable to green ground cover in those areas at that date. For the 2015 classification, the overall accuracies for all areas were over 90%. The areas with the lowest User accuracy were A and B, which contained pre-existing vegetation. Potential causes of error included shadows being commissioned into the woody cover class or woody cover not being detected in shadows in the reference data. The area with lowest Producer accuracy was E (84%). For the 2016, overall classification accuracies for all areas were above 90% apart from A (Table 12), while no User accuracy was below 90%, the lowest Producer accuracies were for areas A and C (83% each).

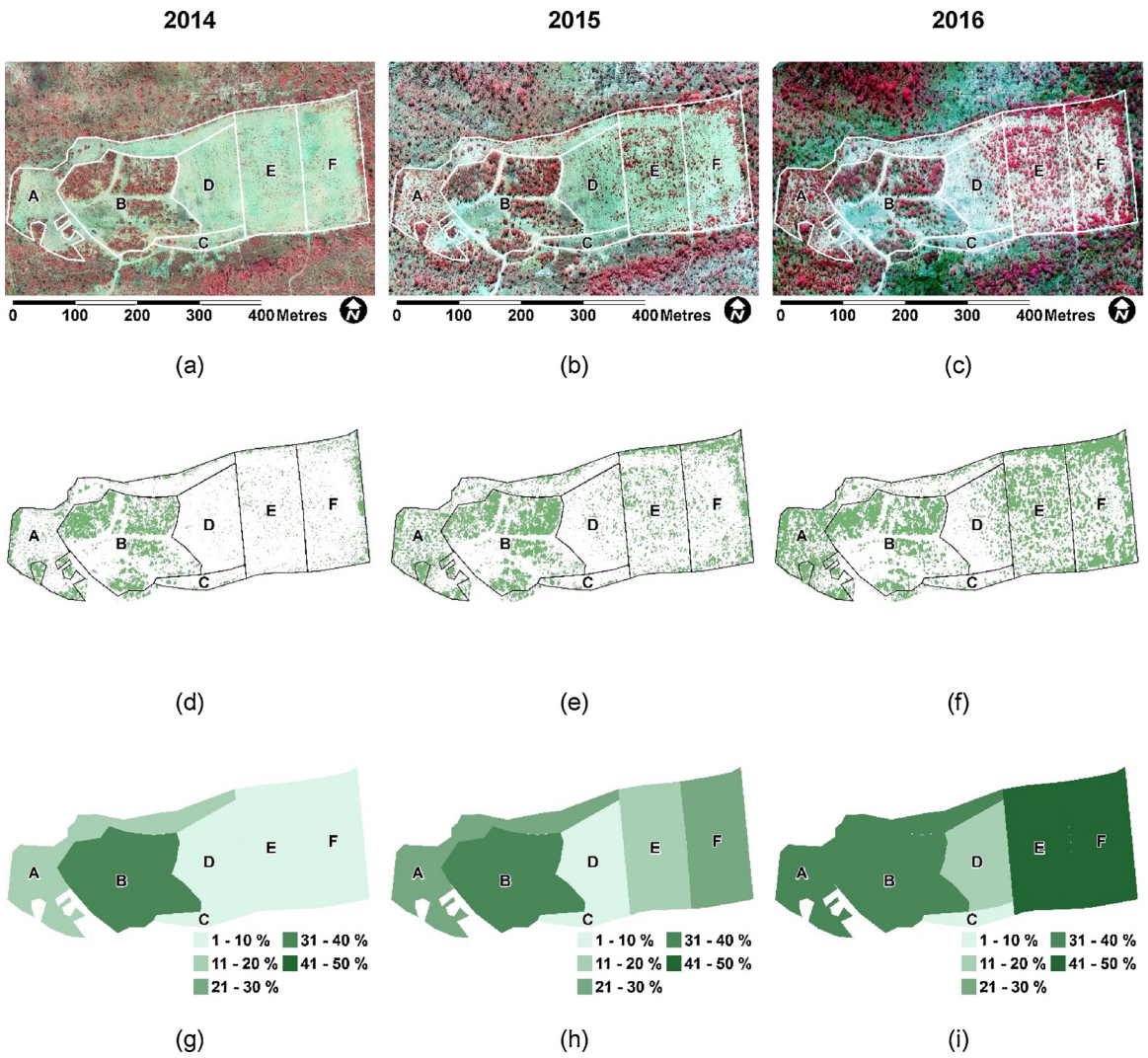

Fig. 7. Mosaics of Sony RGB and NIR images for 23 December 2014 (a) and 10 July 2015 (b). MicaSense RedEdge image for 1 June 2016 (c). NIR, Red and Green bands are shown in RGB space. Woody cover (shown in green) for each of the three dates (d–f). Proportional cover per planting area for each date (g–i). (For interpretation of the references to colour in this figure legend, the reader is referred to the web version of this article).

Table 7
Confusion matrix for 2014 woody cover classification.

Classified	Reference Woody	Non woody	Sum	User Accuracy	Commission error
Woody	170	8	178	96 %	4%
Non woody cover	5	567	572	99 %	1%
Sum	175	575	750		
Producer Accuracy	97%	99%		Overall Accuracy	98 %
Omission error	3%	1%			

Table 8
Confusion matrix for 2015 woody cover classification.

Classified	Reference Woody	Non woody	Sum	User Accuracy	Commission error
Woody	203	17	220	92%	8%
Non woody	15	515	530	97%	3%
Sum	218	532	750		
Producer Accuracy	93%	97%		Overall Accuracy	96%
Omission error	7%	3%			

3.3. Proportional cover per planting area

All but one of the planting areas showed an increase in proportional cover over the three dates (Fig. 9). Only one planting area displayed a reduction in cover (area B) between 2015 and 2016 although not enough to change class (Fig. 7g–i). Given only 15 plants were planted in this area, the reduction in cover between 2015 and 2016 will most likely have been in some mortality of pre-existing vegetation. The two areas with the largest change in cover are areas E and F (increasing from 4% and 7% to 41% and 43% respectively). Areas C and D have the lowest proportional cover for all three dates (15% or less) although planting area D does change to a higher proportion class between 2015 and 2016 (Fig. 7i). A contributing factor to the low cover could be most of planting areas C and D have noticeable slope and exposed substrate (waste rock) as much of the finer surface material (sand) has moved down hill to planting areas E and F. While providing an assessment of performance per planting area analysis at that scale does not provide the resolution to indicate whether change is consistent across the entire planting area.

Table 9
Confusion matrix for 2016 woody cover classification.

Classified	Reference Woody	Non woody	Sum	User Accuracy	Commission error
Woody	278	16	294	95%	5%
Non woody	23	433	456	95%	5%
Sum	301	449	750		
Producer Accuracy	92%	96%		Overall Accuracy	95%
Omission error	8%	4%			

3.4. Proportional cover per cell

Proportional cover for each date per 10 × 10 m square cell at the L2 level are shown in Fig. 10. Scatterplots showing regression between woody cover extracted from the object-based technique and manually derived means are shown in Fig. 11. The r^2 values were 0.95, 0.89 and 0.85 for 2014, 2015 and 2016 respectively. Proportional cover increases are most noticeable around the periphery of the study area suggesting recruitment of volunteers from adjacent areas with natural vegetation. Between the three dates, there has been an increase in the number of cells in the highest three classes, 31– 40%', '41– 50%' and 'Greater than 50%'. The respective increases are 26%, 34% and 44% between 2014 and 2015, and 46%, 43% and 86% between 2015 and 2016. In corroboration with the above results, across the three dates there is a decrease in the number of cells in the classes '1 to 10%' and '11 to 20%'. Between 2014 and 2015, the number of cells in these classes decreased 31% and 7% respectively. Between 2015 and 2016, the number of cells in these classes decreased by 44% and 18% respectively.

Analysis of change in class per 10 × 10 m cell for the three dates shows most cells either stayed in the same class or shifted to a class with a higher proportion of cover (Fig. 12). Between 2014 and 2015, 658 cells changed to a denser class, 408 remained in the same class and 86 changed to a class with less proportional cover (Fig. 12a). Between 2015 and 2016, 604 cells changed to a class with higher proportional cover, 435 remained in the same class and 113 changed to a class with lower proportional cover (Fig. 12b). Most cells that changed to a lower proportional cover were in areas with pre-exisiting vegetation or on areas with slopes and waste rock near the surface.

4. Discussion

During this study, woody cover estimates were successfully extracted from multispectral RPAS data with different dates, spatial and radiometric properties, enabling quantitative change analysis. This work shows RPAS technologies are an effective method for collecting ultra-high spatial resolution multispectral data needed to provide information at the appropriate scales (Laliberte et al., 2011a; Lucieer et al., 2012).

The differences in the geometric accuracy between the Pix4D processed orthophoto mosaics were less than 1 pixel making the data ideal for high spatial resolution change detection. Although, there was no geometric accuracy information supplied with the commercially produced orthomosaic, it was registered to geometrically corrected imagery by the photogrammetric company.

Table 10
Summary of overall, User and Producer accuracies for each planting area for 2014.

Area	Overall accuracy (%)	User accuracy (%)	Producer accuracy (%)
A	99	100	97
B	98	100	97
C	98	100	91
D	98	83	100
E	96	80	100
F	100	100	100

Table 11
Summary of overall, User and Producer accuracies for each planting area for 2015.

Area	Overall accuracy (%)	User accuracy (%)	Producer accuracy (%)
A	91	82	89
B	91	87	92
C	97	95	88
D	98	100	89
E	92	98	84
F	99	98	100

Table 12
Summary of overall, User and Producer accuracies for plant for each planting area for 2016.

Area	Overall accuracy (%)	User accuracy (%)	Producer accuracy (%)
A	88	97	83
B	95	93	93
C	96	95	83
D	97	94	94
E	98	97	100
F	94	90	97

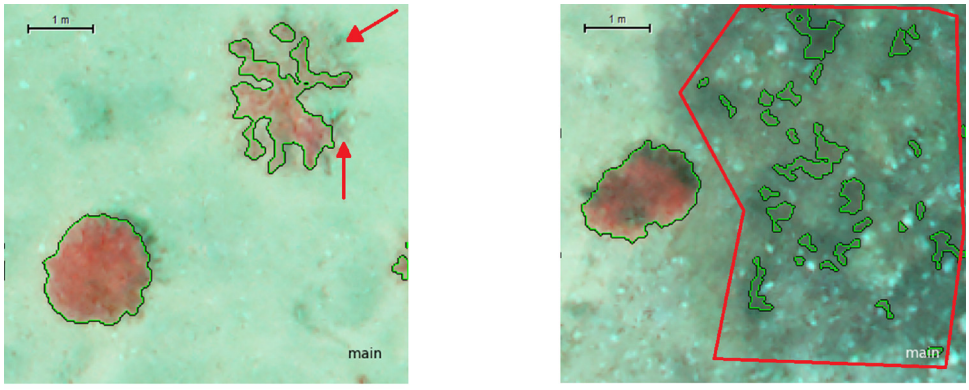

(a) (b)

Fig. 8. Examples of omission and commission from the December 2014 classification. Areas of omission are indicated using red arrows in (a). Objects of commission found within the red polygon in (b). (For interpretation of the references to colour in this figure legend, the reader is referred to the web version of this article).

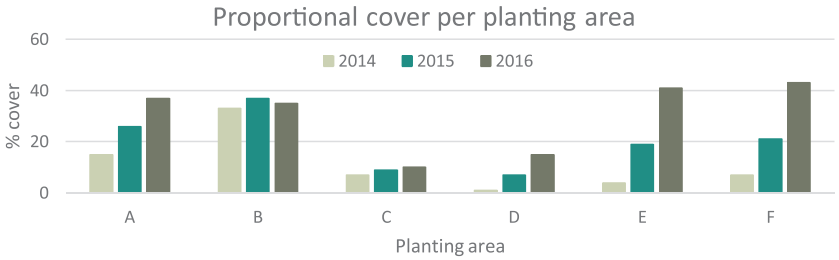

Fig. 9. Proportional cover per planting area for each of the three dates.

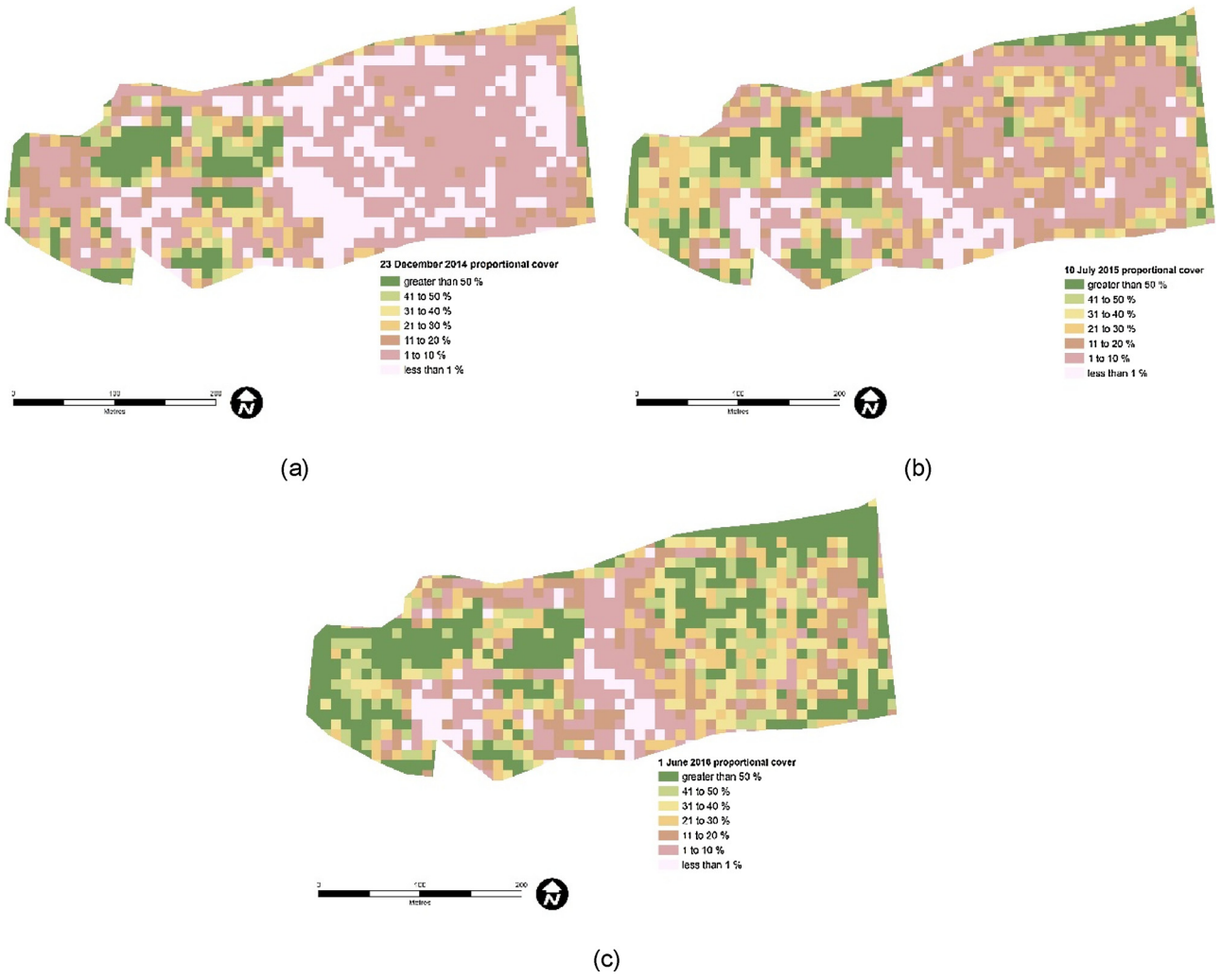

Fig. 10. Maps of proportional woody cover per 10 x 10 m cell for 23 December 2014 (a), 10 July 2015 (b) and 1 June 2016 (c).

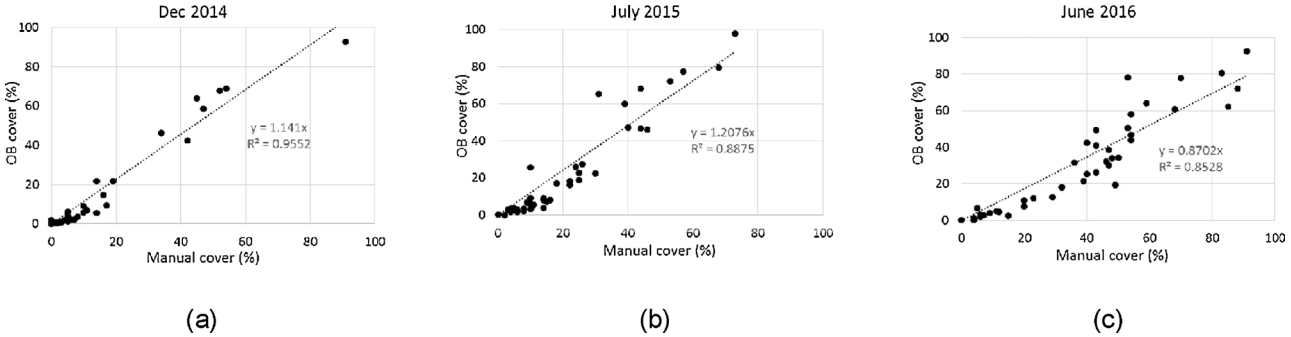

Fig. 11. Scatterplots showing regression between percentage cover derived from object-based technique and manually derived estimates for 2014(a), 2015 (b) and 2016 (c).

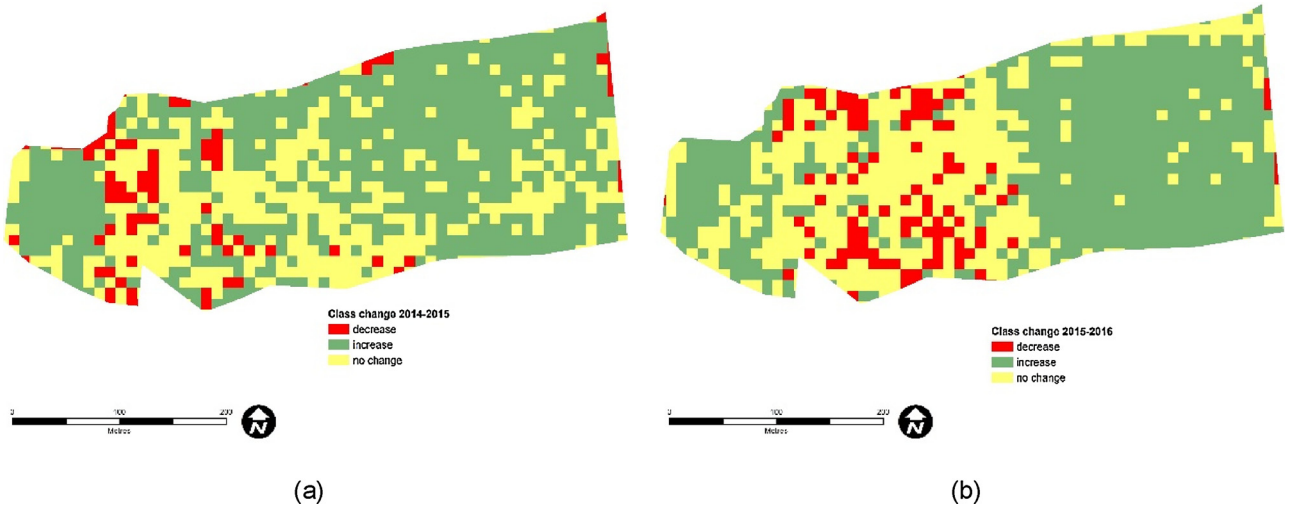

Fig. 12. Changes in class between 2014–2015 (a), and 2015–2016 (b).

The data collected provides the ability to undertake whole of site assessment of woody cover. By analysing the entire site, this eliminated issues surrounding plot based method of data collection such as uncertainty introduced by sampling bias and the possibility of missing change information not in the plots. The quantitative 2D measures of woody cover can be applied to time series data to analyse change in woody cover over the entire site, and is thus suitable for assessing the performance of a revegetation program. The technique works well on data produced by different processing methods, and of varying radiometric quality and spatial resolution. These data can be analysed at scales relevant to monitoring of mine site revegetation, such as whole of site, per planting area or other arbitrary scales. There are benefits in using a scale of objects between individual plants and the planting areas for analysing woody cover. Although only an arbitrary spatial unit, the 10×10 m cell objects provide an assessment of proportional cover across the site at a scale that is capable of detecting fine scale change. The strong linear relationship between object-based proportional woody cover and the manually derived cover estimates shows that this method is an effective means for collecting woody cover information over an entire site. The detection of change at the appropriate scale enables the focus of management activities on targeted areas that require remediation. Larger objects such as the planting areas (L3 in the analysis) do not provide adequate spatial detail to detect fine scale change. For example, planting area D increased in cover over the three dates, however this increase was confined to the eastern portion of the area. The western portion remained relatively unchanged and this was not detected at the L3 level analysis.

A major strength of this technique for object-based woody cover detection is that it can be applied to data sets of different radiometric and geometric qualities. This was achieved firstly, by slightly adjusting the value of the segmentation NDVI threshold parameter to account for the radiometric differences between sensors and secondly, by using object size parameters based on metric units in preference to number of pixels. Despite the different radiometric qualities of the data, the technique worked well with both the narrow spectral bandwidth of the MicaSense bands, the broader overlapping bands of Sony images. The technique was also successful despite peak responses for red and NIR bands in Sony imagery (606 nm and 740 nm, respectively) being different to the central wavelengths of red and NIR in the MicaSense imagery (660 nm and 840 nm, respectively). This was partially achieved by converting DNs to surface reflectance and using the NDVI for extracting woody cover.

In addition, the technique worked well on all data sets despite the GSD differences. The slightly lower overall accuracy of the 2016 classification may have been a result of the coarser GSD. Pixels within the MicaSense RedEdge mosaic are over four times the area of pixels in the Sony mosaics. The only geometric adjustment to the technique between the data sets were rules based upon pixel size. Any rules based on size needed the per-pixel area to be four times less for the MicaSense RedEdge data. The impact on data analysis was minimal given that the GSD in both cases was much less than the objects under investigation. Differences in the detail of plant borders due to different pixel sizes may largely be overcome by the application of the low pass Gaussian filter reducing noise.

One limitation of the technique is that it does not attempt species discrimination. Using a single spectral index limits the ability to do this, particularly when investigating juvenile plants with very similar spectral responses. Species discrimination should be possible with the further application of some other indices, the incorporation of hyperspectral data, the use of textural and context information of the objects (Laliberte and Rango, 2009), and structural information such as derived from 3D point clouds from either photogrammetric or LiDAR data (Wallace et al., 2016). In addition, the technique does not identify non-photosynthetic vegetation. Being based upon an index that detects green vegetation, it does not detect senescent or dead plants.

Another limitation with the technique is sparse vegetation may not be detected in some instances due to the influence of background through the canopy. This can result in the incorrect delineation of tree crowns particularly toward the edge of the tree crown. In addition, there were some instances where the technique was not able to differentiate between woody cover and photosynthetic ground cover. The impact of this limitation was minimised due to the existence of very little ground cover upon the site in any of the three orthomosaics. In addition, using imagery that optimises the difference in reflectance between canopy and ground cover from the dry season should increase the effectiveness of the technique. Most of the ground cover in the region is either annual or perennial in nature and canopy is either semi- or non-deciduous, so using NDVI based on imagery captured only during the dry season (May-October) would enable successful detection of woody cover.

Structural information, including canopy height, which could potentially be derived from the DSM created during photogrammetric processing was not considered for analysis in this study due to a lack of detection of numerous canopies from the 2015 and 2016 data sets. In addition, no DSM was available for the 2014 data. Factors affecting the canopy from appearing in the point cloud used to create DSMs are related to both the canopy structure of the plants on the site and weather conditions. Many of the plants have erectophile (vertically-angled) leaves and sparse canopies with influence from below canopy background even at 3 cm GSD. In addition, the plants were young with

flexible stems resulting in mobile canopies in windy conditions. Automatic tie point identification within canopies that are moving in the wind can fail. This highlights a compromise in timing between ideal lighting conditions for imagery capture and wind speed. The best lighting conditions for capturing imagery for vegetation analysis are in the middle of the day when the sun is near zenith such as with the three data sets used in this study. However, this is also the time of day when the wind is highest. The best wind conditions (little to none) for capturing still canopies are either in the early morning or late afternoon when shadows are long and lighting conditions are less than optimal. The use of an RPAS-mounted LiDAR sensor to collect 3D data would be one way to overcome the limitations using photogrammetric point clouds for vegetation structural information (Wallace et al., 2016).

5. Conclusion

An RPAS was used to collect multispectral imagery over a remote rehabilitated mine site. A robust, semi-automated object-based technique was developed to extract woody cover from the site for the purpose of the provision of information for analysing the success of the revegetation effort. The technique was successful at extracting woody cover from the spatially and radiometrically different data sets gathered. The object-based technique will now be applied to all datasets collected approximately every three months over the mine site between 2014 and 2017. A more detailed multi-temporal analysis of woody cover change will be conducted over that time frame. The woody cover objects from the time series will undergo further change analysis including the application of object fate metrics (after Browning et al., 2011) to gain an understanding of the temporal dynamics of woody cover on an establishing revegetation site. As the revegetation establishes further, ongoing monitoring will be conducted at a coarser temporal scale (annual to biennial). The method developed in this project will be applied to monitor other ongoing mine site rehabilitation in the region specifically the nearby Ranger uranium mine.

References

Armston, J.D., Denham, R.J., Danaher, T.J., Scarth, P.F., Moffiet, T.N., 2009. Prediction and validation of foliage projective cover from Landsat-5 TM and Landsat-7 ETM+ imagery. J. Appl. Remote Sens. 3 (1), 033540.

Bao, N., Lechner, A., Fletcher, A., Erskine, P., Mulligan, D., Bai, Z., 2014. Spoting long-term changes in vegetation over short-term variability. Int. J. Min. Reclam. Environ. 28 (1), 2–24.

Blaschke, T., 2010. Object based image analysis for remote sensing. ISPRS J. Photogramm. Remote Sens. 65, 2–16.

Booth, D.T., Cox, S.E., 2009. Dual-camera, high-resolution aerial assessment of pipeline revegetation. Environ. Monit. Assess. 158, 23–33.

Breckenridge, R.P., Dakins, M., Bunting, S., Harbour, J.L., White, S., 2011. Comparison of unmanned aerial vehicle platforms for assessing vegetation cover in sagebrush steppe ecosystems. Rangel. Ecol. Manage. 64 (5), 521–532.

Browning, D.M., Laliberte, A.S., Rango, A., 2011. Temporal dynamics of shrub proliferation: linking patches to landscapes. Int. J. Geogr. Inform. Sci. 25 (6), 913–930.

Bryson, M., Johnson-Roberson, M., Murphy, R.J., Bongiorno, D., 2013. Kite aerial photography for low-cost, ultra-high spatial resolution multi-spectral mapping of intertidal landscapes. PLoS One 8 (9), e73550.

Chabot, D., Bird, D.M., 2013. Small unmanned aircraft: precise and convenient new tools for surveying wetlands. J. Unmanned Veh. Syst. 1 (01), 15–24.

Chabot, D., Dillon, C., Ahmed, O., Shemrock, A., 2017. Object-based analysis of UAS imagery to map emergent and submerged invasive aquatic vegetation: a case study. J. Unmanned Veh. Syst. 5 (1), 27–33.

Chen, J.M., Rich, P.M., Gower, S.T., Norman, J.M., Plummer, S., 1997. Leaf area index of boreal forests: theory techniques, and measurements. J. Geophys. Res. 102 (D24) 29429-29443.

Congalton, R.G., Green, K., 2009. Assessing the Accuracy of Remotely Sensed Data: Principles and Practices, 2nd ed. CRC Press, Boca Raton, Fl.

Curran, P.J., Foody, G.M., 1994. The use of remote sensing to characterise the regenerative states of tropical forests. In: Foody, G.M., Curran, P.J. (Eds.), Environmental Remote Sensing from Regional to Global Scales. John Wiley, Chichester, pp. 44–83.

d'Oleire-Oltmanns, S., Marzolff, I., Peter, K.D., Ries, J.B., 2012. Unmanned Aerial Vehicle (UAV) for monitoring soil erosion in Morocco. Remote Sens. 4 (11), 3390–3416.

d'Oleire-Oltmanns, S., Eisank, C., Drăgut, L., Blaschke, T., 2013. An object-based workflow to extract landforms at multiple scales from two distinct data types. IEEE Geosci. Remote Sens. Lett. 10 (4), 947–951.

Dufour, S., Bernez, I., Betbeder, J., Corgne, S., Hubert-Moy, L., Nabucet, J., Rapinel, S., Sawtschuk, J., Trollé, C., 2013. Monitoring restored riparian vegetation: how can recent developments in remote sensing sciences help? Knowl. Manag. Aquat. Ecosyst. 410 (10), 15.

Dunford, R., Michel, K., Gagnage, M., Piégay, H., Trémelo, M.L., 2009. Potential and constraints of Unmanned Aerial Vehicle technology for the characterization of Mediterranean riparian forest. Int. J. Remote Sens. 30 (19), 4915–4935.

Fensham, R.J., Fairfax, R.J., Holman, J.E., Whitehead, P.J., 2002. Quantitative assessment of vegetation structural attributes from aerial photography. Int. J. Remote Sens. 23 (11), 2293–2317.

Field, S.A., O'Connor, P.J., Tyre, A.J., Possingham, H.P., 2007. Making monitoring meaningful. Austral Ecol. 32 (5), 485–491.

Gardner, T.A., Barlow, J., Araujo, I.S., TC, Ávila-Pires, Bonaldo, A.B., Costa, J.E., Esposito, M.C., Ferreira, L.V., Hawes, J., Hernandez, M.I., 2008. The cost-effectiveness of biodiversity surveys in tropical forests. Ecol. Lett. 11 (2), 139–150.

Getzin, S., Wiegand, K., Schöning, I., 2012. Assessing biodiversity in forests using very high-resolution images and unmanned aerial vehicles. Methods Ecol. Evol. 3 (2), 397–404.

Gitelson, A.A., 2004. Wide dynamic range vegetation index for remote quantification of biophysical characteristics of vegetation. J. Plant Physiol. 161 (2), 165–173.

Gravina, A., McKenna, P., Glenn, V., 2011. Evaluating the success of mineral sand mine rehabilitation on North stradbroke Island, Queensland: comparisons with reference eucalypt communities. Proceedings of the Royal Society of Queensland 117, 419–435.

Harwin, S., Lucieer, A., 2012. Assessing the accuracy of georeferenced point clouds produced via multi-view stereopsis from unmanned aerial vehicle (UAV) imagery. Remote Sens. 4 (6), 1573–1599.

Hung, C., Sukkarieh, S., 2013. Robotic aircraft and intelligent surveillance systems for weed detection. Plant Protect. Q. 28 (3), 78.

Hunt, E.R., Doraiswamy, P.C., McMurtrey, J.E., Daughtry, C.S., Perry, E.M., Akhmedov, B., 2013. A visible band index for remote sensing leaf chlorophyll content at the canopy scale. Int. J. Appl. Earth Obs. Geoinf. 21, 103–112.

Husson, E., Hagner, O., Ecke, F., 2014. Unmanned aircraft systems help to map aquatic vegetation. Appl. Veg. Sci. 17 (3), 567–577.

Hutley, L.B., Beringer, J., Isaac, P.R., Hacker, J.M., Cernusak, L.A., 2011. A sub-continental scale living laboratory: spatial patterns of savanna vegetation over a rainfall gradient in northern Australia. Agric. For. Meteorol. 151, 1417–1428.

Kelcey, J., Lucieer, A., 2012. Sensor correction of a 6-band multispectral imaging sensor for UAV remote sensing. Remote Sens. 4 (5), 1462–1493.

Kelcey, J., Lucieer, A., 2013. An adaptive texture selection framework for ultra-high resolution UAV imagery. IEEE International Geoscience and Remote Sensing Symposium-IGARSS. IEEE. pp. 3883–3886.

Koh, L., Wich, S., 2012. Dawn of drone ecology: low-cost autonomous aerial vehicles for conservation. Trop. Conserv. Sci. 5 (3), 121–132.

Laliberte, A.S., Rango, A., 2009. Texture and scale in object-based analysis of sub-decimeter resolution unmanned aerial vehicle (UAV) imagery. IEEE Trans. Geosci. Remote Sens. 47 (3), 761–770.

Laliberte, A.S., Rango, A., 2011. Image processing and classification procedures for analysis of sub-decimeter imagery acquired with an unmanned aircraft over arid rangelands. GIScience Remote Sens. 48 (1), 4–23.

Laliberte, A.S., Herrick, J.E., Rango, A., Winters, C., 2010. Acquisition, orthorectification, and object-based classification of unmanned aerial vehicle (UAV) imagery for rangeland monitoring. Photogramm. Eng. Remote Sens. 76 (6), 661–672.

Laliberte, A.S., Goforth, M.A., Steele, C.M., Rango, A., 2011a. Multispectral remote sensing from unmanned aircraft: image processing workflows and applications for rangeland environments. Remote Sens. 3 (11), 2529–2551.

Laliberte, A.S., Winters, C., Rango, A., 2011b. UAS remote sensing missions for rangeland applications. Geocarto Int. 26 (2), 141–156.

Lechner, A., Arnold, S., Fletcher, A., Gordon, A., Erskine, P., Gillespie, M., Mulligan, D., 2012a. Embracing modern ecological methods: monitoring and modelling for mine closure not compliance. In: Proc. Life of Mine Conference Brisbane. Australia 10-12 July.

Lechner, A., Fletcher, A., Johansen, K., Erskine, P., 2012b. Characterising upland swamps using object-based classification methods and hyper-spatial resolution imagery derived from an unmanned aerial vehicle. Proceedings of the XXII ISPRS Congress Annals of the Photogrammetry, Remote Sensing and Spatial Information Sciences. pp. 101–106.

Lelong, C.C., Burger, P., Jubelin, G., Roux, B., Labbé, S., Baret, F., 2008. Assessment of unmanned aerial vehicles imagery for quantitative monitoring of wheat crop in small plots. Sensors 8 (5), 3557–3585.

Lisein, J., Pierrot-Deseilligny, M., Bonnet, S., Lejeune, P., 2013. A photogrammetric workflow for the creation of a forest canopy height model from small unmanned aerial system imagery. Forests 4 (4), 922–944.

López-Granados, F., 2011. Weed detection for site-specific weed management: mapping and real-time approaches. Weed Res. 51 (1), 1–11.

Lu, B., He, Y., Liu, H.H.T., 2017. Mapping vegetation biophysical and biochemical properties using unmanned aerial vehicles-acquired imagery. Int. J. Remote Sens. 1–23.

Lucieer, A., Robinson, S., Turner, D., Harwin, S., Kelcey, J., 2012. Using a micro-UAV for ultra-high resolution multi-sensor observations of Antarctic moss beds. Int. Arch. Photogramm XXXIX-B1, 429–433.

Mayr, M.J., Malß, S., Ofner, E., Samimi, C., 2017. Disturbance feedbacks on the height of woody vegetation in a savannah: a multi-plot assessment using an unmanned aerial vehicle (UAV). Int. J. Remote Sens. 1–25.

McGwire, K.C., Weltz, M.A., Finzel, J.A., Morris, C.E., Fenstermaker, L.F., McGraw, D.S., 2013. Multiscale assessment of green leaf cover in a semi-arid rangeland with a small

unmanned aerial vehicle. Int. J. Remote Sens. 34 (5), 1615–1632.
Mildrexler, D.J., Zhao, M., Heinsch, F.A., Running, S.W., 2007. A new satellite-based methodology for continental-scale disturbance detection. Ecol. Appl. 17 (1), 235–250.
Murwira, A., Skidmore, A.K., 2006. Monitoring change in the spatial heterogeneity of vegetation cover in an African savanna. Int. J. Remote Sens. 27 (11), 2255–2269.
Pádua, L., Vanko, J., Hruška, J., Adão, T., Sousa, J.J., Peres, E., Morais, R., 2017. UAS, sensors, and data processing in agroforestry: a review towards practical applications. Int. J. Remote Sens. 38 (8-10), 2349–2391.
Peña, J.M., Torres-Sánchez, J., de Castro, A.I., Kelly, M., López-Granados, F., 2013. Weed mapping in early-season maize fields using object-based analysis of unmanned aerial vehicle (UAV) images. PLoS One 8 (10), e77151.
Pfitzner, K., Staben, G., Bartolo, R., 2010. The spectral reflectance of common artificial pseudo invariant materials. In: Proceedings of the 15th Australasian Remote Sensing and Photogrammetry Conference. Alice Springs 13-17 September.
Puliti, S., Ørka, H.O., Gobakken, T., Næsset, E., 2015. Inventory of small forest areas using an unmanned aerial system. Remote Sens. 7 (8), 9632–9654.
Rasmussen, J., Nielsen, J., Garcia-Ruiz, F., Christensen, S., Streibig, J.C., 2013. Potential uses of small unmanned aircraft systems (UAS) in weed research. Weed Res. 53 (4), 242–248.
Reed, B.C., Brown, J.F., VanderZee, D., Loveland, T.R., Merchant, J.W., Ohlen, D.O., 1994. Measuring phenological variability from satellite imagery. J. Veg. Sci. 5 (5), 703–714.
Rouse, J.W., Haas, R.H., Schell, J.A., Deering, D.W., 1973. Monitoring vegetation systems in the Great plains with ERTS. In: 3rd ERTS Symposium. NASA, Washington. pp. 309–317.
Sankey, T.T., Donager, J., McVay, J., Sankey, J.B., 2017. UAV lidar and hyperspectral fusion for forest monitoring in the southwestern USA. Remote Sens. Environ. 195, 30–43.
Simioni, G., Gignoux, J., Le Roux, X., 2003. Tree layer spatial structure can affect savanna production and water budget: results of a 3-D model. Ecology 84 (7), 1879–1894.
Smith, G.M., Milton, E.J., 1999. The use of the empirical line method to calibrate remotely sensed data to reflectance. Int. J. Remote Sens. 20 (13), 2653–2662.
Specht, R.L., 1981. Foliage projective cover and standing biomass. In: Gillison, A.N., Anderson, D.J. (Eds.), Vegetation Classification in Australia: Proceedings of a Workshop Sponsored by CSIRO Division of Land Use Research. CSIRO and ANU Press, Canberra. October, 1978.
Staben, G.W., Lucieer, A., Evans, K.G., Scarth, P., Cook, G.D., 2016. Obtaining biophysical measurements of woody vegetation from high resolution digital aerial photography in tropical and arid environments: Northern Territory, Australia. Int. J. Appl. Earth Obs. Geoinf. 52 204-220.ss.
Stagakis, S., González-Dugo, V., Cid, P., Guillén-Climent, M.L., Zarco-Tejada, P.J., 2012. Monitoring water stress and fruit quality in an orange orchard under regulated deficit irrigation using narrow-band structural and physiological remote sensing indices. ISPRS J. Photogramm. Remote Sens. 71, 47–61.
Strecha, C., Fletcher, A., Lechner, A., Erskine, P., Fua, P., 2012. Developing species specific vegetation maps using multi-spectral hyperspatial imagery from unmanned aerial vehicles. ISPRS Ann. Photogramm I-3, 311–316.
Suárez, L., Zarco-Tejada, P.J., González-Dugo, V., Berni, J.A.J., Sagardoy, R., Morales, F., Fereres, E., 2010. Detecting water stress effects on fruit quality in orchards with time-series PRI airborne imagery. Remote Sens. Environ. 114 (2), 286–298.
Van Iersel, W.K., Straatsma, M., Addink, E., Middelkoop, H., 2016. Monitoring phenology of floodplain grassland and herbaceous vegetation with UAV imagery. Proc. XXIII ISPRS Congress, Commission VII, 12–19 July 2016, Prague, Czech Republic. International Society for Photogrammetry and Remote Sensing. pp. 569–571.
Wallace, L., Lucieer, A., Malenovský, Z., Turner, D., Vopěnka, P., 2016. Assessment of Forest structure using Two UAV techniques: a comparison of airborne laser scanning and structure from motion (SfM) Point clouds. Forests 7 (3), 62.
Whiteside, T.G., Bartolo, R.E., 2015. Use of WorldView-2 time series to establish a wetland monitoring program for potential offsite impacts of mine site rehabilitation. Int. J. Appl. Earth Obs. Geoinf. 42 (0), 24–37.
Zarco-Tejada, P.J., González-Dugo, V., Berni, J.A.J., 2012. Fluorescence, temperature and narrow-band indices acquired from a UAV platform for water stress detection using a micro-hSyperspectral imager and a thermal camera. Remote Sens. Environ. 117, 322–337.